Nanoscale

Voltage-Reduced Low-Defect Graphene Oxide: A High Conductivity, Near-Zero Temperature Coefficient of Resistance Material

Journal:	*Nanoscale*
Manuscript ID	NR-COM-10-2018-008285.R1
Article Type:	Communication
Date Submitted by the Author:	21-Nov-2018
Complete List of Authors:	Silverstein, Kevin; Binghamton University, Physics, Applied Physics and Astronomy Halbig, Christian; Freie Universität Berlin Mehta, Jeremy; Binghamton University Sharma, Anju; Binghamton University Eigler, Siegfried; Freie Universität Berlin Mativetsky, Jeffrey; Binghamton University, Physics, Applied Physics and Astronomy

Journal Name

COMMUNICATION

Voltage-Reduced Low-Defect Graphene Oxide: A High Conductivity, Near-Zero Temperature Coefficient of Resistance Material†

Received 00th January 20xx,
Accepted 00th January 20xx

DOI: 10.1039/x0xx00000x

www.rsc.org/

Kevin W. Silverstein,[a] Christian E. Halbig,[b] Jeremy S. Mehta,[a] Anju Sharma,[c] Siegfried Eigler,[b] Jeffrey M. Mativetsky*[a]

A highly conductive graphene derivative was produced by using a low-defect form of graphene oxide, oxo-G, in conjunction with voltage-reduction, a simple and environmentally-benign procedure for removing oxygen-containing functional groups. A low temperature coefficient of resistance was achieved, making this material promising for temperature-stable electronics and sensors.

Graphene oxide (GO) is a versatile two-dimensional nanomaterial which, unlike graphene, is easily processed from aqueous suspensions. GO has recently been explored for its many useful properties such as photoluminescence, high mechanical strength, tunable conductivity, tunable interactions with chemical species, and as a precursor for graphene-based derivatives.[1–6] These properties allow GO to serve as a key component in a wide range of applications such as: composite materials,[7] supercapacitors,[8] rain and sun powered solar cells,[9] drug delivery platforms,[10] and chemical/biological sensors.[11] Many applications, however, require temperature-stable performance, for example in manufacturing, automotive, and aerospace industries.[12,13] Temperature stable materials have been used to improve the performance of tactile sensor arrays for robotic hands and used for temperature independent oxygen sensors for control of engine exhaust.[14,15] Inducing temperature-stable characteristics in GO-based materials would therefore broaden the function of GO.

The tunable properties of GO stem from its polydisperse structure. GO consists of a hexagonal carbon lattice, whereby nanoscale aromatic sp^2 carbon domains are separated by sp^3 hybridized regions bearing covalently bound oxo-functional groups such as epoxides, hydroxyls, and organosulfates along the basal plane, and hydroxyl, carboxyl and carbonyl groups along sheet edges.[16,17] These functional groups, along with lattice vacancies, disrupt the conductive sp^2 carbon network, rendering GO electrically insulating.[18] The chemical, optical, and electrical properties of GO can be modified, however, through various reduction schemes, e.g., chemical,[19,20] thermal,[21] photo-induced,[18] or electrochemical.[19] GO reduction removes oxygen-containing functional groups resulting in a restoration of the sp^2 carbon network. The extent of the sp^2 carbon lattice restoration is dependent on the reduction method and the initial integrity of the hexagonal carbon framework.

Voltage-reduction has recently emerged as a "green" alternative that enables reduction under ambient conditions without the use of chemical reagents,[22–25] produces reduced GO (rGO) with oxygen removal levels that are comparable with more cumbersome or hazardous methods,[24] and can be used for patterning nanoscale conductive pathways.[26] Nevertheless, the continuity of the restored sp^2 lattice following reduction (by all methods) is still far from that of graphene, limiting the use of rGO for electronic applications. Moreover, the strongly temperature-dependent resistance of voltage- (and conventionally) reduced GO limits use in sensors.[24,27,28]

To enhance the electrical performance of rGO, there have been efforts to lower the density of lattice vacancies that are introduced during GO synthesis. Harsh synthesis conditions, for example when using the typical Hummer's method, cause the formation of vacancies through the evolution of CO and CO_2. Eigler *et al.* showed that extended oxidation times at low temperatures can inhibit decomposition reactions, leading to a low-defect form of GO, referred to as oxo-functionalized graphene (oxo-G).[29] Based on Raman spectroscopy and high-resolution transmission electron microscopy, it was shown that oxo-G, when chemically reduced, has a highly preserved carbon framework with an extremely low vacancy defect density, as low as 0.01%.[29–33] With its significantly more intact carbon framework, using oxo-G as a precursor for voltage

[a] Department of Physics, Applied Physics, and Astronomy, Binghamton University, Binghamton, NY 13902, USA.
[b] Institute of Chemistry and Biochemistry, Freie Universität Berlin, Takustraße 3, 14195 Berlin, Germany.
[c] Small Scale Systems Integration and Packaging Center, Binghamton University, Binghamton, NY 13902, USA.
* Email: jmativet@binghamton.edu
† Electronic Supplementary Information (ESI) available: Oxo-G sheet size and film thickness, oxo-G reduction, and variable temperature measurements. See DOI: 10.1039/x0xx00000x

reduction should lead to a high conductivity material.

Here we present the voltage reduction of oxo-G as a means of generating highly-conductive voltage-reduced oxo-G (V-roxo-G). The resulting material is 48 times more conductive than conventional voltage-reduced GO (V-rGO). In addition, over a broad temperature range, a near-zero temperature coefficient of resistance is observed, making V-roxo-G promising for electronics and sensing devices that require a temperature-stable response.

Oxo-G was chemically derived from graphite by using a previously published protocol.[5,29] Briefly, graphite (1 g) was suspended in 24 mL of sulfuric acid (98%) at 4 °C and then oxidized for 16 hrs following the addition of potassium permanganate over 4 hrs. A glycol/water bath with an immersed refrigerating coil was used to maintain the temperature below 10 °C and minimize CO_2 formation. While still below 10 °C, 20 mL of cold H_2SO_4 (20%, over 4 hrs), 100 mL of cold H_2O (over 16 hrs) and 40 mL of hydrogen peroxide (5%) were added, whereby the latter agent was used to make the manganese salts soluble. The final product was purified by repetitive centrifugation and exfoliated by pulsed tip sonication. After redispersion in water at a concentration of 1.85 mg/ml, the material was stored at 4 °C.

Glass substrates were cleaned by sonication in acetone, isopropyl alcohol, and water, followed by UV-ozone treatment. Electrode pairs with 200 and 500 µm gaps were patterned by thermally evaporating 3 nm of Cr and 50 nm of Au through a shadow mask. The oxo-G suspension was stirred at room temperature for 2-3 hrs and drop-casted onto the substrates to form 40 to 150 nm thick films, depending on the volume cast. The samples were dried under ambient conditions for 12 hrs and then transferred to a humidity-controlled glovebox at 70% relative humidity (RH) for over 24 hrs. Oxo-G within the electrode gap regions was fully reduced by applying a voltage across electrode pairs, 2 V for 5 hrs followed by 4 V for 1 hr at 70% RH. The reduction was recorded *in situ* under an optical microscope. Local V-roxo-G film thickness at each electrode gap was measured using atomic force microscopy.

Electrical conductivity was measured under nitrogen using a Keithley 2425 SourceMeter and a four-point probe setup to eliminate contact resistance. Raman spectroscopy was performed using a Renishaw inVia confocal Raman microscope with a 532 nm, 47.2 mW laser focused to a 0.87 µm spot; 625 spectra were recorded over a 22.5 µm x 22.5 µm sample area using a 0.9 µm step size and a minimally-invasive laser dose to maintain sample integrity (integration time = 1 s, laser intensity = 8×10^6 W/m^2).[34] X-ray photoelectron spectroscopy (XPS) was performed using a PHI 5000 VersaProbe in ultrahigh vacuum (10^{-7} Pa). A 50 W monochromatic Al Kα (1486.6 eV) X-ray source was used to acquire spectra using a 200 µm spot size. XPS spectra were calibrated to the sp^2-bonded carbon peak (284.5 eV). Variable temperature electrical measurements were performed with a four-point configuration under vacuum with an Oxford Instruments Heliox Cryostat.

As shown in Fig. 1a, oxo-G was reduced between Au electrode pairs by applying a voltage across the electrodes. The voltage reduction is expected to follow the same reaction

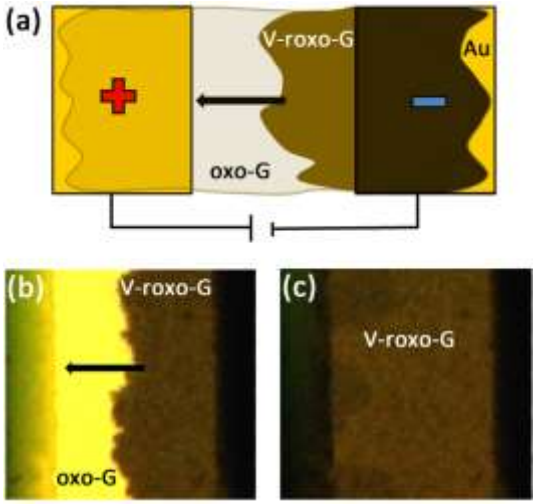

Fig. 1. (a) Top view of setup for reducing oxo-G between two Au electrodes. Optical microscope image showing (b) the reduction process at 2 V after 3 hours, with a V-roxo-G growth front moving from right to left, and (c) following complete reduction. The oxo-G on top of the Au electrodes also darkens due to reduction.

pathway proposed for GO.[22,24] Namely, hydrolysis of adsorbed water near the positive electrode generates H^+, electrons, and O_2; the H^+ is then transferred, e.g. by Grotthuss diffusion, through the adsorbed water, along the electric field, towards the negative electrode where oxo-G reduction occurs. As reduction proceeds, the resulting conductive V-roxo-G front effectively extends the negative electrode until the electrode pair is bridged by V-roxo-G. *In situ* measurements of the growth can be seen in Fig. 1b which shows a brown V-roxo-G front proceeding from the negative to positive electrode until the entire electrode gap is filled (Fig. 1c). Although voltage reduction resembles electrochemical reduction in its chemical pathway, it is a distinctly different process since the substrate is not immersed in an electrolyte. Instead, the reduction is enabled by adsorbed water that is present on GO, and oxo-G, under ambient or humid conditions.[35]

One advantage of voltage reduction is that the electrodes used for reduction can also serve as contacts for subsequent electrical characterization, or for device integration.[23] The four point conductivity of V-roxo-G was measured to be 380 ± 20 S/cm, 48 times higher than the conductivity of V-rGO. This conductivity for V-roxo-G exceeds that found for chemically-reduced GO and approaches the performance of GO reduced under extreme conditions, e.g., combined treatment with hydrazine for 24 hrs followed by thermal reduction at 1100 °C under Ar/H_2 (see Table 1). Unlike the chemical treatments, however, voltage-reduction results in no waste products, and unlike high-temperature processes, voltage-reduction is compatible with plastic substrates.

Reduction Method	Conductivity (S/cm)
Voltage (V-roxo-G)	380 ± 20
Voltage (V-rGO)[24]	8
Hydrazine[21]	10
Vitamin C[36]	80
Hydroiodic Acid[37]	300
Hydrazine + 1100 °C under Ar/H_2[21]	550

Table 1. Conductivity of V-roxo-G compared with literature values for rGO.

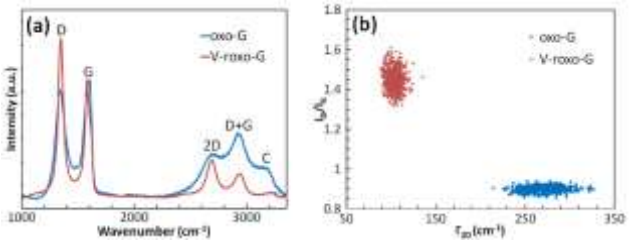

Fig. 2. Raman spectroscopy performed on oxo-G and V-roxo-G. (a) Raman spectra averaged over 625 sample locations, normalized to the G band intensity, showing an increase in the D band and a decrease in the 2D band width after reduction. (b) Ratio of the D band and G band intensity versus 2D band width.

Fig. 2a shows average Raman spectra for oxo-G and V-roxo-G, each compiled from 625 spectra recorded under minimally invasive laser conditions.[34] The D and G bands are prominent at 1350 cm^{-1} and 1580 cm^{-1}, respectively. The D band is associated with the phonon breathing modes of the carbon rings and the G band is associated with degenerate E_{2G} phonon modes of sp^2 carbon bonds.[38] Less prominent bands, 2D, D+G, and C, are also observed at higher wavenumbers. Following reduction, the D band decreases in intensity (along with the D+G and C bands) with respect to the G band, and the width of the 2D band narrows. The G band also narrows, making the D' band become visible as a shoulder of the G band.

The ratio of the D and G band intensity (I_D/I_G) can be related to the mean distance between lattice defects (L_D), while the width of the 2D band is commonly used to gauge lattice disorder.[39] To determine whether the V-roxo-G is in the low-disorder (Tuinstra–Koenig) or disordered regime,[40] we analysed the dependence of I_D/I_G on the 2D width (Fig. 2b). An I_D/I_G ratio that decreases with decreasing 2D width indicates that the material is in the low-disorder regime and I_D/I_G is proportional to L_D, while an I_D/I_G ratio that increases with decreasing 2D width indicates that the material is in the disordered regime and I_D/I_G is proportional to L_D^2:[38]

$$\frac{I_D}{I_G} = (0.55\ \mathrm{nm}^{-2})L_D^2. \qquad (1)$$

It can be seen in Fig. 2b that, upon reduction of oxo-G, the 2D band width decreases on average from 270 ± 20 cm^{-1} to 104 ± 6 cm^{-1}, while I_D/I_G increases from 0.91 ± 0.02 to 1.44 ± 0.09, meaning that V-roxo-G is in the disordered regime. The distribution of the clustered data points represents the variations in local structure between sample positions. Using equation 1, we find that L_D increases from 1.28 to 1.62 nm following voltage reduction, corresponding to an increase in the average sp^2 carbon domain size, from 54 to 87 carbon atoms. Previously, GO was found to have an I_D/I_G of 0.87 ± 0.02, with an increase to 0.95 ± 0.04 following voltage reduction, corresponding to a modest increase in average sp^2 carbon domain size from 52 to only 57 carbon atoms.[24]

For insight into changes in the chemical makeup of oxo-G following voltage reduction, XPS was performed, as shown in Fig. 3. The C1s spectrum was deconvoluted into five components: sp^2, sp^3, C-O, C=O, and COOH at 284.5, 285.3, 286.7, 288.0, and 288.9 eV, respectively (all ± 0.2 eV). Prior to reduction, oxo-G shows a prominent C-O peak and a prominent peak composed of sp^2 and sp^3 carbon components. After

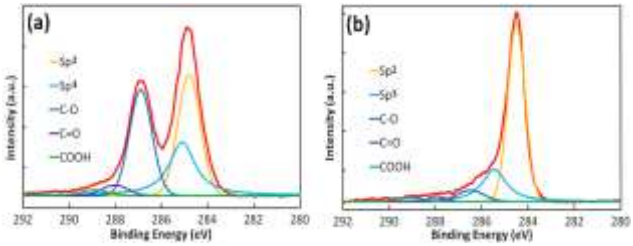

Fig. 3. Deconvoluted C 1s core XPS spectra of (a) pristine oxo-G and (b) V-roxo-G.

reduction, V-roxo-G exhibits a dramatic drop in C-O peak intensity.

The overall decrease in oxygen concentration was determined from the areas under the O1s and C1s spectra, yielding an oxygen concentration of 22 at% for oxo-G, which decreases to 7 at% after reduction. For comparison, this residual oxygen concentration is much lower than that for V-rGO (12%),[24] and lower than the residual oxygen level for GO reduced at 1100 °C under ultrahigh vacuum (8%).[21] Combining voltage-induced reduction with a low-defect starting material therefore allows for a highly-reduced end product.

In addition to increasing the conductivity within individual sheets, the high reduction level in V-roxo-G could also benefit charge transport between overlapping V-roxo-G sheets. The XPS measurements reveal that V-roxo-G contains fewer protruding oxygen-containing functional groups than V-rGO, while Raman spectroscopy shows larger sp^2 domains in V-roxo-G. Taken together, these results suggest that sp^2 regions in overlapping V-roxo-G sheets are better able to come into close contact with each other than V-rGO sheets, in turn decreasing the inter-sheet resistance.

The charge transport mechanism in V-roxo-G was investigated by measuring film resistance as temperature was varied from 16 K to 373 K. Across this entire temperature range, current-voltage curves were ohmic. As shown in Fig. 4a, the resistance increases with decreasing temperature. In general, the temperature-dependent resistance for rGO can be fit to $R(T) = R_0 \exp(T_0/T)^p$, with exponent p depending on the specific transport mechanism. To determine p, the reduced activation energy W can be found using [27,41,42]

$$W = -\frac{\partial \ln R(T)}{\partial \ln T} = p(T_0/T)^p. \qquad (2)$$

By plotting the natural log of the reduced activation energy versus the natural log of temperature, exponent p is given by the slope. As shown in Fig. 4b, using this approach for temperatures of 16K to 75K, a linear fit yields a p value of 0.43. Efros-Shklovskii variable range hopping (ES-VRH) exhibits p = 1/2 [41] while two-dimensional Mott Variable range hopping (2D-VRH) exhibits p =1/3.[43] Previously, V-rGO was found to nearly follow ES-VRH (p = 0.46), which is associated with the nanoscale sp^2 carbon domains acting as a disordered array of quantum dots that localize the charge carriers.[44] V-roxo-G, with p = 0.43 below 75 K, is intermediate between ES-VHR and 2D-VRH, suggesting reduced coulombic interactions compared

with V-rGO due to increased connectivity between sp^2 domains.

Surprisingly, above 75 K, an unusually low p value of 0.03 is obtained, meaning that there is a minimal change in resistance with temperature. A 20% decrease in resistance is seen

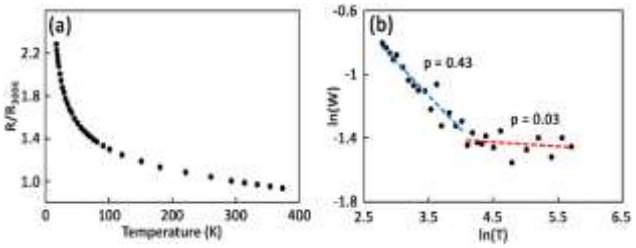

Fig. 4. (a) Normalized V-roxo-G resistance as a function of temperature. (b) Natural log of the reduced activation energy versus natural log of temperature. A linear fit for each regime is shown with its corresponding slope value, p.

between 180 and 373 K and only a 7% decrease between 292 and 373 K. This minimal dependence of resistance on temperature has implications for sensors and other electronics that need to be insensitive to temperature changes. For this reason, many studies have gone to great lengths to induce a low temperature coefficient of resistance (TCR). For example, Lipomi *et al.* used graphene-metal composites to achieve a low TCR,[45] and Zhu *et al.* used graphene-GO hybrids with varying degrees of reduction.[46] In most cases, a low TCR is achieved by combining and balancing the contributions of materials with negative and positive TCRs, e.g. semiconducting and metallic components. Interestingly, in our case, only one material is needed. While V-roxo-G still exhibits a slightly negative TCR, it may feature sp^2 domains that are approaching a semimetallic character as their size and connectivity increase, providing a positive TCR contribution to the overall response. In other words, the heterogeneous structure of V-roxo-G, with residual oxygen-containing groups and defects, leads to variable-range hopping, negative TCR behavior; however, the emergence of highly intact sp^2 regions results in local positive TCR contributions. Overall, the balance of both contributions is a relatively flat temperature response.

The TCR can be evaluated using:

$$\mathrm{TCR} = \mathrm{R}_0^{-1}\left(\frac{\partial \mathrm{R}}{\partial \mathrm{T}}\right), \qquad (3)$$

where R_0 is a reference temperature (typically 292 K). Using equation 3 with R_0 = 292 K, the TCR was found to be -0.0009 K^{-1} over a range of 292 K to 373 K and -0.0011 K^{-1} over a range of 180K to 373K. These TCR values are comparable with other low TCR materials such as nichrome, manganin, graphite, and ruthenium-oxide-titanium-oxide composites.[46,47] Moreover, unlike other graphene-based low-TCR materials, V-roxo-G avoids the need for multi-component composites, chemical vapor deposition, or graphene transfer. Instead, a low TCR is achieved by solution deposition followed by a simple, environmentally benign processing of a single nanomaterial.

In summary, the voltage reduction of oxo-G produces a highly conductive, two-dimensional material that is 48 times more conductive than conventional V-rGO and rivals the conductivity of GO reduced under extreme thermal or chemical conditions. Following voltage reduction, a substantially lowered oxygen content and restored sp^2 network result in a temperature-dependent resistance below 75 K that indicates increased charge delocalization relative to V-rGO, and a nearly-temperature independent behavior at temperatures above 75 K. The low TCR, high electrical conductivity, and simple, green processing of V-roxo-G make it promising for wearable sensors and flexible electronics that require temperature-stable performance.

We acknowledge support from the National Science Foundation (CMMI-1537648). This work made use of Binghamton University's Analytical and Diagnostics Laboratory and facilities acquired through the National Science Foundation Major Research Instrumentation Program (CMMI-1429176). We also thank Bruce White for access and assistance with his cryostat system.

Conflicts of interest

There are no conflicts to declare.

Notes and references

1 W. Wei and X. Qu, *Small*, 2012, **8**, 2138.
2 S. Eigler and A. Hirsch, *Angew. Chemie - Int. Ed.*, 2014, **53**, 7720.
3 A. K. Geim and K. S. Novoselov, *Nat. Mater.*, 2007, **6**, 183.
4 S. Pei and H. M. Cheng, *Carbon*, 2012, **50**, 3210.
5 C. E. Halbig, O. Martin, F. Hauke, S. Eigler and A. Hirsch, *Chem. - A Eur. J.*, DOI:10.1002/chem.201802500.
6 H. Pieper, C. E. Halbig, L. Kovbasyuk, M. R. Filipovic, S. Eigler and A. Mokhir, *Chem. - A Eur. J.*, 2016, **22**, 15389.
7 S.-H. Oh, K.-R. Kim, J.-M. Yun and P. H. Kang, *Phys. Status Solidi*, 2015, **212**, 376.
8 J. Xu, Z. Tan, W. Zeng, G. Chen, S. Wu, Y. Zhao, K. Ni, Z. Tao, M. Ikram, H. Ji and Y. Zhu, *Adv. Mater.*, 2016, **28**, 5222.
9 Q. Tang, X. Wang, P. Yang and B. He, *Angew. Chemie - Int. Ed.*, 2016, **55**, 5243.
10 Z. Liu, J. T. Robinson, X. Sun and H. Dai, *J. Am. Chem. Soc.*, 2008, **130**, 10876.
11 W. Xuan, M. He, N. Meng, X. He, W. Wang, J. Chen, T. Shi, T. Hasan, Z. Xu, Y. Xu and J. K. Luo, *Sci. Rep.*, 2014, **4**, 7206.
12 S. Shafeie, S. Guo, P. Erhart, Q. Hu and A. Palmqvist, *Adv. Mater.*, https://doi.org/10.1002/adma.201805392.
13 V. Balakrishnan, H.-P. Phan, T. Dinh, D. Dao and N.-T. Nguyen, *Sensors*, 2017, **17**, 2061.
14 M. Sohgawa, D. Hirashima, Y. Moriguchi, T. Uematsu, W. Mito, T. Kanashima, M. Okuyama and H. Noma, *Sensors Actuators, A Phys.*, 2012, **186**, 32.
15 R. Moos, W. Menesklou, H.-J. Schreiner and K. Heinz Hardtl, *Sensors Actuators, B Chem.*, 2000, **67**, 178.
16 A. Lerf, H. He, M. Forster and J. Klinowski, *J. Phys. Chem. B*, 1998, **102**, 4477.
17 D. R. Dreyer, S. Park, C. W. Bielawski and R. S. Ruoff, *Chem. Soc. Rev.*, 2010, **39**, 228.
18 Y. G. Bi, J. Feng, Y. F. Li, Y. L. Zhang, Y. S. Liu, L. Chen, Y. F. Liu, L. Guo, S. Wei and H. B. Sun, *ACS Photonics*, 2014, **1**, 690.
19 V. S. Dilimon and S. Sampath, *Thin Solid Films*, 2011, **519**, 2323.
20 S. Eigler, S. Grimm, M. Enzelberger-Heim, P. Müller and A. Hirsch, *Chem. Commun.*, 2013, **49**, 7391.
21 C. Mattevi, G. Eda, S. Agnoli, S. Miller, K. A. Mkhoyan, O. Celik, D. Mastrogiovanni, G. Granozzi, E. Carfunkel and M. Chhowalla, *Adv. Funct. Mater.*, 2009, **19**, 2577.

22 J. M. Mativetsky, E. Treossi, E. Orgiu, M. Melucci, G. P. Veronese, P. Samorì and V. Palermo, *J. Am. Chem. Soc.*, 2010, **132**, 14130.
23 J. M. Mativetsky, A. Liscio, E. Treossi, E. Orgiu, A. Zanelli, P. Samorì and V. Palermo, *J. Am. Chem. Soc.*, 2011, **133**, 14320.
24 A. C. Faucett, J. N. Flournoy, J. S. Mehta and J. M. Mativetsky, *FlatChem*, 2017, **1**, 42.
25 M. C. C. Morant-Miñana, J. Heidler, G. Glasser, H. Lu, R. Berger, N. Gil-Gonzalez, K. Muellen, D. de Leeuw and K. Asadi, *Mater. Horizons*, DOI:10.1039/C8MH00895G.
26 A. C. Faucett and J. M. Mativetsky, *Carbon N. Y.*, 2015, **95**, 1069.
27 D. Joung, L. Zhai and S. Khondaker, *Phys. Rev. B*, 2011, **83**, 115323.
28 G. Eda, C. Mattevi, H. Yamaguchi, H. Kim and M. Chhowalla, *J. Phys. Chem. C*, 2009, **113**, 15768.
29 S. Eigler, M. Enzelberger-Heim, S. Grimm, P. Hofmann, W. Kroener, A. Geworski, C. Dotzer, M. Röckert, J. Xiao, C. Papp, O. Lytken, H. P. Steinrück, P. Müller and A. Hirsch, *Adv. Mater.*, 2013, **25**, 3583.
30 S. Seiler, C. E. Halbig, F. Grote, P. Rietsch, F. Börrnert, U. Kaiser, B. Meyer and S. Eigler, *Nat. Commun.*, 2018, **9**, 836.
31 P. Feicht and S. Eigler, *ChemNanoMat*, 2018, **4**, 244.
32 F. Grote, C. Gruber, F. Börrnert, U. Kaiser and S. Eigler, *Angew. Chemie - Int. Ed.*, 2017, **56**, 9222.
33 S. Eigler, *Chem. Commun.*, 2015, **51**, 3162.
34 J. S. Mehta, A. C. Faucett, A. Sharma and J. M. Mativetsky, *J. Phys. Chem. C*, 2017, **121**, 16584.
35 H. Bi, K. Yin, X. Xie, J. Ji, S. Wan, L. Sun, M. Terrones and M. S. Dresselhaus, *Sci. Rep.*, 2013, **3**, 2714.
36 M. J. Fernández-Merino, L. Guardia, J. I. Paredes, S. Villar-Rodil, P. Solís-Fernández, A. Martínez-Alonso and J. M. D. Tascón, *J. Phys. Chem. C*, 2010, **114**, 6426.
37 S. Pei, J. Zhao, J. Du, W. Ren and H. M. Cheng, *Carbon*, 2010, **48**, 4466.
38 A. C. Ferrari and D. M. Basko, *Nat. Nanotechnol.*, 2013, **8**, 235.
39 L. G. Cançado, A. Jorio, E. H. M. Ferreira, F. Stavale, C. A. Achete, R. B. Capaz, M. V. O. Moutinho, A. Lombardo, T. S. Kulmala and A. C. Ferrari, *Nano Lett.*, 2011, **11**, 3190.
40 M. M. Lucchese, F. Stavale, E. H. M. Ferreira, C. Vilani, M. V. O. Moutinho, R. B. Capaz, C. A. Achete and A. Jorio, *Carbon*, 2010, **48**, 1592.
41 D. Joung and S. I. Khondaker, *Phys. Rev. B*, 2012, **86**, 235423.
42 J. M. Mativetsky and W. R. Datars, *Phys. B*, 2002, **324**, 191.
43 A. B. Kaiser, G. N. Cristina, R. S. Sundaram, M. Burghard and K. Kern, *Nano Lett.*, 2009, **9**, 1787.
44 K. C. Beverly, J. F. Sampaio and J. R. Heath, *J. Phys. Chem. B*, 2002, **106**, 2131.
45 B. C. Marin, S. E. Root, A. D. Urbina, E. Aklile, R. Miller, A. V. Zaretski and D. J. Lipomi, *ACS Omega*, 2017, **2**, 626.
46 P. Sun, M. Zhu, K. Wang, M. Zhong, J. Wei, D. Wu and H. Zhu, *ACS Appl. Mater. Interfaces*, 2013, **5**, 9563.
47 D. C. Giancoli, *Physics*, Prentice Hall, 6th Ed., 2005.

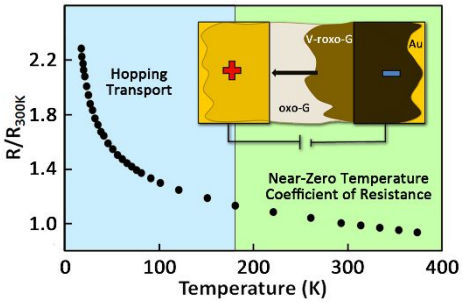

A highly conductive, low temperature coefficient of resistance nanomaterial was generated by using low-defect graphene oxide in conjunction with voltage-reduction.